

*Short Communication*

## **Preparation of Carbon- Based Composite NiO/MoO<sub>2</sub>/MoO<sub>3</sub>/C by Electrodeposition and Its Application in Microbial Electrolysis Cells**

Yu Zhao\*, Yuxue Wang, Ailian Wu, Jia Li

College of Chemistry and Chemical Engineering, Taiyuan University of Technology, Taiyuan, Shanxi, P. R. China, 030024

\*E-mail: [zhaoyu@tyut.edu.cn](mailto:zhaoyu@tyut.edu.cn)

*Received:* 5 May 2019 / *Accepted:* 11 July 2019 / *Published:* 5 August 2019

---

In this paper, a NiO/MoO<sub>2</sub>/MoO<sub>3</sub>/C composite was prepared via cyclic voltammetry by using carbon paper as a substrate, and was applied as a cathode material in a microbial electrolysis cell. Scanning electron microscopy was performed to study the lamellar structure of this composite. The x-ray microscopy results revealed the nanocrystalline structure of the composite. While the XPS test results showed that the composite contained Mo<sup>6+</sup>, Mo<sup>4+</sup> and Ni<sup>2+</sup>. Although the electrochemical activity of Mo/Ni was slightly inferior to that of Pt according to the linear sweep voltammetry and Tafel test, its hydrogen production performance was higher than the latter. In addition, Mo/Ni showed an excellent stability.

---

**Keywords:** Microbial electrolysis cell; Composite NiO/MoO<sub>2</sub>/MoO<sub>3</sub>/C; Hydrogen production; Cyclic voltammetry electrodeposition

### **1. INTRODUCTION**

The global demand for energy has led to an increase in the consumption of non-renewable energy sources and the resulting pollution has caused great harm to our living environment. Clean, sustainable and renewable microbial electrolysis cells (MECs) [1-2] have been widely recognised as novel types of hydrogen production technologies. In these cells, the bacteria in the anode decomposes organic matter into protons and electrons that reach the cathode and participate in the hydrogen production process. Therefore, the MEC cathode plays a crucial role in hydrogen production. The traditional cathode material is the noble metal platinum [3]. Given its high price and easy poisoning by wastewater pollutants, the performance of non-platinum cathode materials has become a research hotspot in recent years.

Nickel and nickel alloys are the most promising alternatives to platinum and have received much research attention. Given their excellent electrocatalytic activity, low overpotential, high corrosion resistance, antibacterial activity and low cost, thereby making them excellent MEC cathode materials [4-8]. The nickel alloy catalyst has a better hydrogen evolution performance than the single Ni catalyst, where the Mo/Ni catalyst has a large specific surface area and a low hydrogen evolution overpotential. Manuel et al. [4] performed an in situ synthesis to load NiMo on foamed nickel with a current density of  $10 \text{ mA cm}^{-2}$  at a voltage of 1.38V. Hu et al. [7-8] electrodeposited 0.11 Mo/Ni to 0.1 Mo/Ni onto a carbon cloth via electrodeposition. At an applied voltage of 0.6 V, the hydrogen yield was  $2.1 \text{ m}^3 \text{ day}^{-1} \text{ m}^{-3}$ .

In this study, a composite NiO/MoO<sub>2</sub>/MoO<sub>3</sub>/C was prepared via cyclic voltammetry electrodeposition and was used as the cathode material of the MEC. The morphology and structure of the prepared materials were characterised, and their hydrogen evolution performance, electrochemical properties and cycle stability were tested.

## 2. MATERIALS AND METHODS

### 2.1 Preparation of cathodes

Carbon paper was used as the working electrode, platinum mesh was used as the counter electrode and the Ag/AgCl electrode was used as the reference electrode to construct a three-electrode system. Mo/Ni was electrodeposited on the carbon paper via cyclic voltammetry. The voltage was set to  $-0.8 \text{ V} - 0\text{V}$ , the sweep speed was  $100 \text{ mV s}^{-1}$ , cyclic voltammetry test 300 laps and then rinsed repeatedly with deionised water. The plating solution for preparing Mo/Ni included:  $40 \text{ g L}^{-1}$  of NiSO<sub>4</sub>·6H<sub>2</sub>O,  $25 \text{ g L}^{-1}$  of Na<sub>2</sub>MoO<sub>4</sub>·2H<sub>2</sub>O and  $45 \text{ g L}^{-1}$  of C<sub>6</sub>H<sub>5</sub>Na<sub>3</sub>O<sub>7</sub>·2H<sub>2</sub>O. The solution was subsequently adjusted to pH 10 with ammonia water.

### 2.2 MEC reactor construction

The single-chamber MEC was constructed by using Plexiglas with a total volume of 100 mL and filled with 20 mL of activated sludge from a local coking wastewater treatment plant (Taiyuan, China). The 80 mL phosphate buffer solution contained  $5.618 \text{ g L}^{-1}$  of Na<sub>2</sub>HPO<sub>4</sub>·12H<sub>2</sub>O;  $6.155 \text{ g L}^{-1}$  of NaH<sub>2</sub>PO<sub>4</sub>·12H<sub>2</sub>O;  $1 \text{ g L}^{-1}$  of glucose;  $20 \text{ mL L}^{-1}$  of trace minerals and PH of 7 (in 1000 mL distilled water). The anode was made of carbon felt ( $2 \times 5 \times 1 \text{ cm}^3$ ) initially inoculated in double-chamber MFCs. A power source (HB 17301 SL; Hossoni, Inc., China) was used to apply 0.7V to the reactors.

### 2.3 Characteristic analysis of cathodes

The surface morphology and structure of the prepared materials were characterised via SEM and XRD. Whilst the valence analysis of the elements was characterised via XPS. The three-electrode system was used to prepare the working electrode, the platinum mesh electrode as the counter electrode and the

Ag–AgCl electrode as the reference electrode. The electrochemical properties of the prepared materials were tested by using an electrochemical workstation. The linear scan range was  $-0.9\text{V}$  to  $0.5\text{V}$ , and the scan rate was  $10\text{ mV s}^{-1}$ . Meanwhile the scan range of the Tafel curve was  $-0.9\text{V}$  to  $0.3\text{V}$ , and its scan rate was  $10\text{ mV s}^{-1}$ . Gas composition was analysed via gas chromatography.

#### 2.4. Calculation

$R_{CE}$  denotes the ratio of the actual electricity generated by the MEC ( $Q$ ) to the theoretical electricity produced by the oxidation of glucose ( $Q_T$ ) and is calculated as  $R_{CE}=Q/Q_T\times 100\%$ ,  $Q = I \times t = \int idt$ ,  $Q_T = F \times b \times \frac{m}{M}$ , where  $I$  is the current generated by the MEC (A);  $F$  is the Faraday (often equal to  $96485\text{ C}\cdot\text{mol}^{-1}$ );  $b=12$ , which represents the amount of electrons lost by 1 mol of  $\text{C}_6\text{H}_{12}\text{O}_6$ ;  $m$  is the mass of  $\text{C}_6\text{H}_{12}\text{O}_6$  consumed; and  $M$  is the molar mass of  $\text{C}_6\text{H}_{12}\text{O}_6$ .

### 3. RESULTS AND DISCUSSION

#### 3.1 Characteristics of NiO/MoO<sub>2</sub>/MoO<sub>3</sub>/C

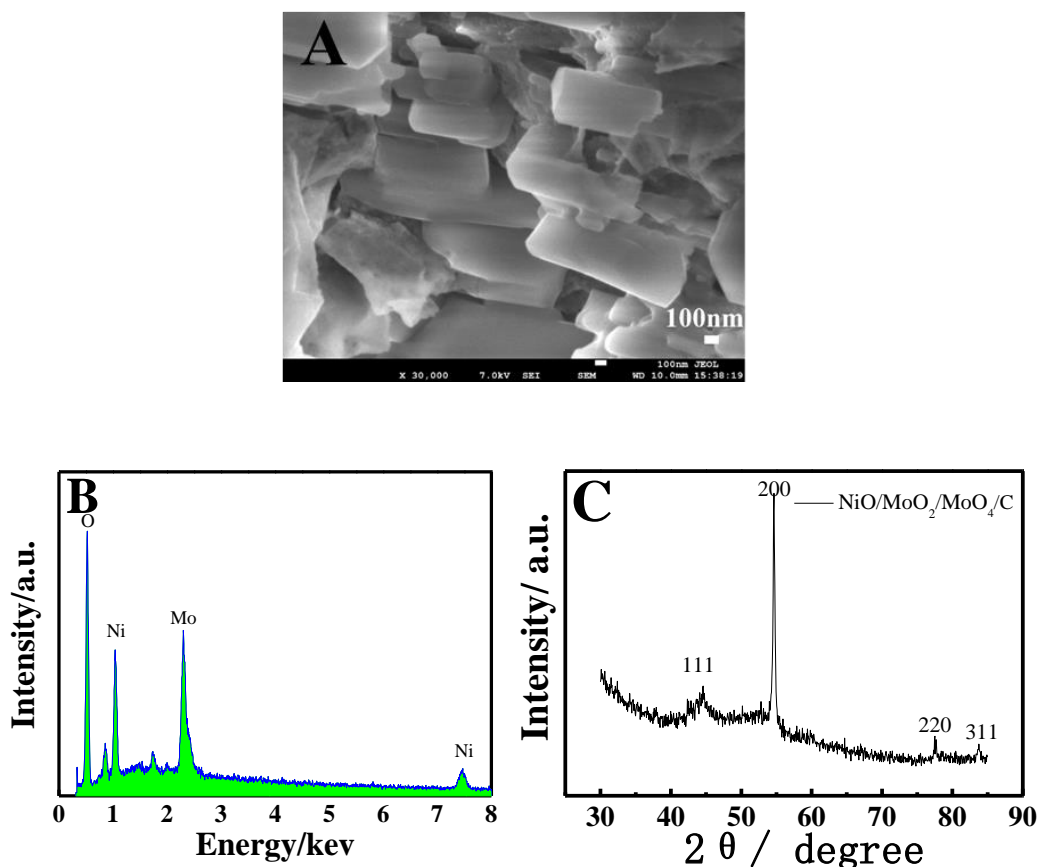


**Figure 1.** Characterisation of NiO/MoO<sub>2</sub>/MoO<sub>3</sub>/C: SEM (A), EDS (B) and XRD (C).

Figure 1 (A) illustrates the SEM of a Mo/Ni material. The NiO/MoO<sub>2</sub>/MoO<sub>3</sub>/C material forms a nanosheet structure with holes between layers. Figure 1 (B) presents an EDS diagram; and shows that the Mo/Ni material mainly contains elements, such as Mo, Ni and O, of which O accounts for 90.4% at most, thereby indicating that an oxide is formed. The crystalline phases of the catalysts characterised by XRD are shown in Figure 1 (C). The crystalline structure of the studied NiO/MoO<sub>2</sub>/MoO<sub>3</sub>/C deposits is affected by two factors, namely, the molybdenum content in NiO/MoO<sub>2</sub>/MoO<sub>3</sub>/C and the Ni content in NiO/MoO<sub>2</sub>/MoO<sub>3</sub>/C. The diffractograms show a broad peak, which indicates that the deposited Mo/Ni has a nanocrystalline structure. The XRD pattern of the deposit with the lowest molybdenum content exhibits the characteristic peaks of the Ni–Mo solid solution FCC structure corresponding to planes (1 1 1), (2 0 0), (2 2 0), (3 1 1) [9].

**Table 1.** NiO/MoO<sub>2</sub>/MoO<sub>3</sub>/C EDS element content

Element	Mass fraction%	Atomic fraction%
O	64.12	90.4
Ni	7.80	3.00
NiO/MoO <sub>2</sub> /MoO <sub>3</sub> /C	28.8	6.60

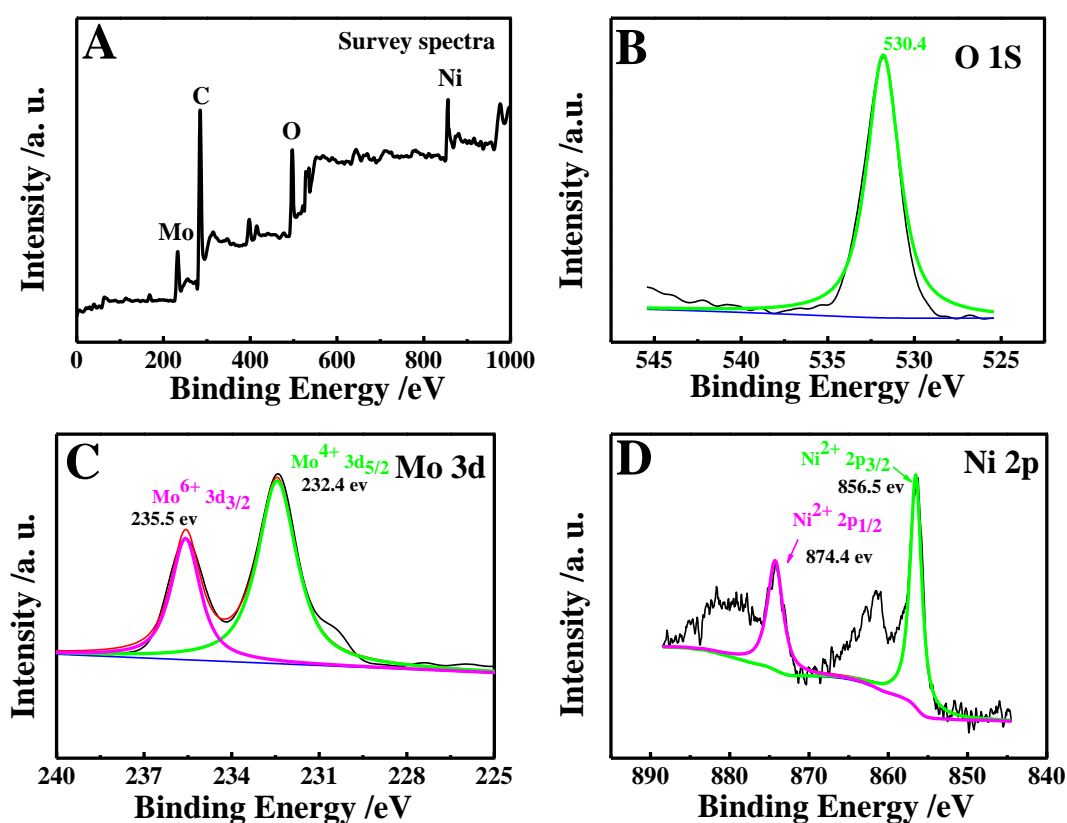


**Figure 2.** XPS spectra of NiO/MoO<sub>2</sub>/MoO<sub>3</sub>/C. (a) Survey spectrum; (b) O1s; (c) Mo3d and (d) Ni2p.

The surface composition of the prepared material and the chemical state of different elements were analysed by XPS. As shown in Figure 2(A), the NiO/MoO<sub>2</sub>/MoO<sub>3</sub>/C cathode material contains Ni,

Mo, C and O elements, which is consistent with the results of the EDS analysis. Figure 2(B) shows the high-resolution XPS spectrum of O 1s. The binding energy of the fitted peak was O<sup>2-</sup> at 530.4 eV, thereby suggesting that the resulting material is an oxide and explaining why the catalyst performance decreases with time [10-11]. Figure 2 (C) presents a high-resolution XPS map of Mo 3d and shows that two fitted peaks were generated. The fitted peak with a binding energy at 232.4 eV represents Mo<sup>4+</sup>3d3/2 [12], whilst the fitted peak at 235.05 eV represents Mo<sup>6+</sup>3d3/2, thereby indicating that Mo<sup>4+</sup> was oxidised to a higher valence state of Mo<sup>6+</sup>, possibly due to MoO<sub>3</sub> [13] or MoO<sub>4</sub><sup>2-</sup> [14]. As shown in Table 1, the ratio of Mo<sup>4+</sup> to Mo<sup>6+</sup> was 2:1. Figure 2(D) shows the high-resolution XPS spectrum of Ni 2p. The two fitted peaks were located at 856.5 eV and 874.4 eV, respectively, representing Ni<sup>2+</sup> [15]. Therefore, the cathode material was a composite NiO/MoO<sub>2</sub>/MoO<sub>3</sub>/C.

**Table 2.** The proportion of two types of molybdenum in the total molybdenum at the surface of NiO/MoO<sub>2</sub>/MoO<sub>3</sub>/C calculated from XPS.

Mo	Mo <sup>4+</sup>	Mo <sup>6+</sup>
Proportion	66.76%	33.24%

### 3.2 Electrochemical performance test

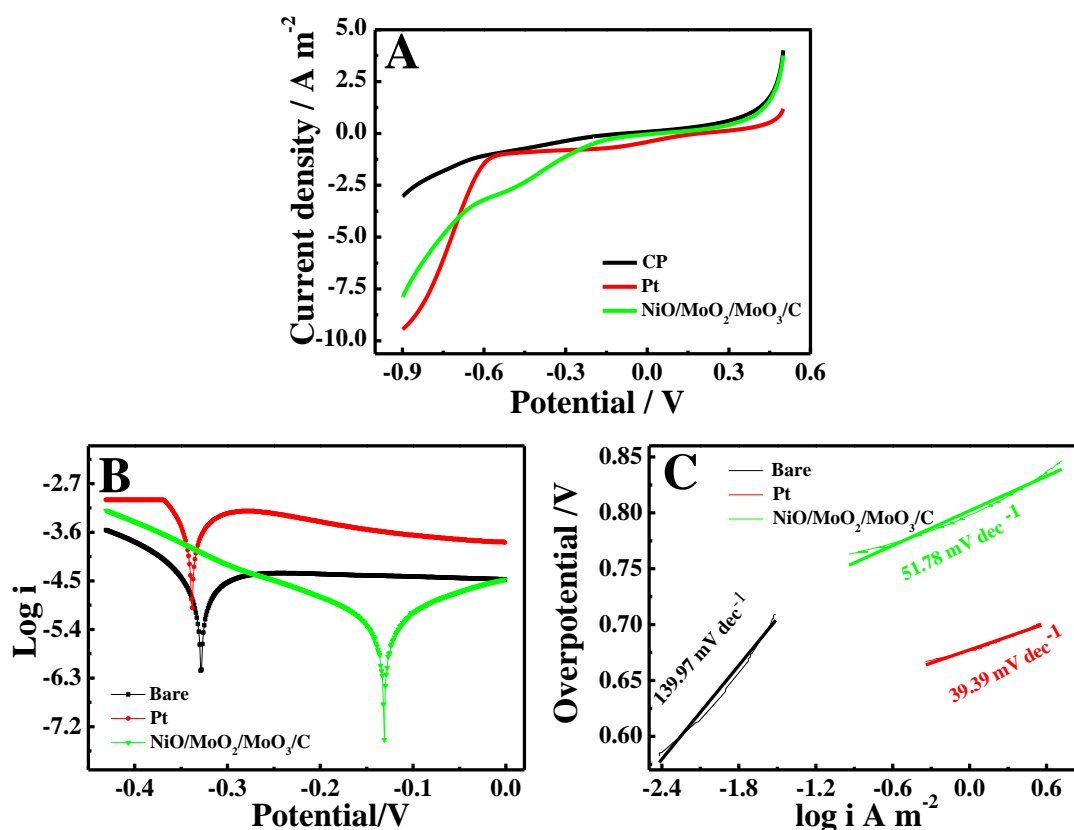


**Figure 3.** Electrochemical performance tests. (A) Linear sweep voltammetry scan range is -0.9 to 0.5 V, and the scan rate is 10 mV s<sup>-1</sup>; (B) Polarization curves were obtained by sweeping the potential from -0.5 V to 0 V at a scan rate of 10 mV s<sup>-1</sup>; (C) The linear fit for the Tafel plots.

We investigated the electrocatalytic HER activities of our NiO/MoO<sub>2</sub>/MoO<sub>3</sub>/C composite material deposited on a carbon paper. As a reference point, we also performed measurements by using a commercial Pt catalyst (20 wt% Pt on Vulcan carbon black) that exhibited high HER catalytic performance. Linear sweep voltammetry (LSV) was used to evaluate the performance of electrochemical hydrogen evolution in different cathodes [16]. From Figure 3(A), the LSV recorded with our NiO/MoO<sub>2</sub>/MoO<sub>3</sub>/C composite on carbon paper electrodes demonstrated a good hydrogen evolution performance, beyond which the cathodic current rapidly increased under highly negative potentials. However, the performance of this composite was inferior to that of Pt. In sharp contrast, bare carbon paper exhibited minimal HER activity. As shown in Figure 3(B), the linear portions of the Tafel plots (Figure 3C) were fitted to the Tafel equation ( $\eta = a + b \log j$ , where  $j$  is the current density and  $b$  is the Tafel slope), thereby yielding Tafel slopes of  $\sim 39.4$ ,  $\sim 51.8$  and  $\sim 140.0$  mV/decade for Pt, the NiO/MoO<sub>2</sub>/MoO<sub>3</sub>/C composite and bare carbon paper, respectively. The Tafel slope is an intrinsic property of the electrocatalyst. A smaller Tafel slope of the catalyst corresponds to a faster hydrogen evolution reaction rate [17].

### 3.3 MEC hydrogen production performance

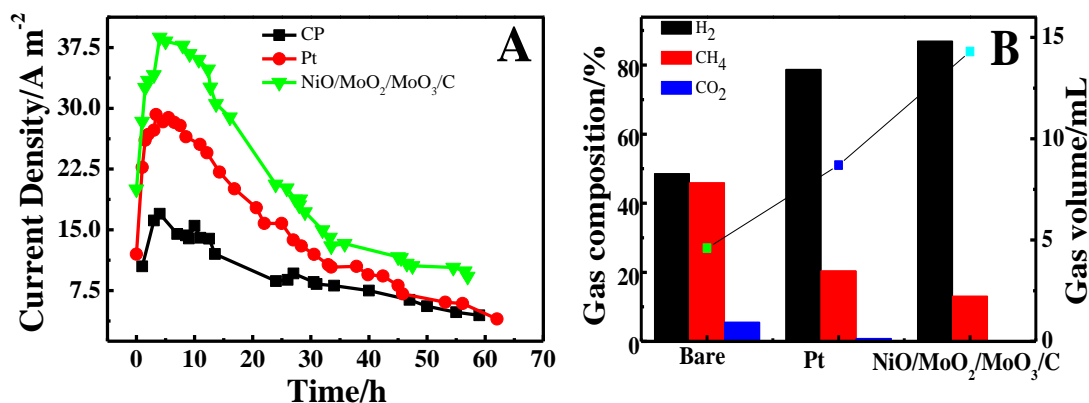


**Figure 4.** Current generation for the three cathode electrodes in the MECs (A) and the MEC gas composition per cycle (B)

The current density was recorded at regular intervals at an applied voltage of 0.7V. The current density increased continuously over time and slowly decrease after about 8 hours probably due to the consumption of the matrix during long-term operation. The current density dropped to 7.5 A m<sup>-2</sup> in about 60 hours. The highest hydrogen production current generated by the NiO/MoO<sub>2</sub>/MoO<sub>3</sub>/C cathode reached 37.5 A m<sup>-2</sup>, which was 1.2 times and 2 times higher than those generated by the Pt cathode blank cathode respectively. At the same applied voltage, it is 144.94% (15.31A m<sup>-2</sup>) higher than that of electrodeposited Ni cathode[18] studied before, and 110.91% (17.78A m<sup>-2</sup>) higher than that of Mg(OH)Cr cathode material studied by Dai et al[19]. Figure 4(B) shows that the NiO/MoO<sub>2</sub>/MoO<sub>3</sub>/C cathode has the largest gas production (14.3mL) and H<sub>2</sub> content of 86.92%, followed by the Pt cathode 9.4 mL with an H<sub>2</sub> content of 67.26% and blank carbon paper generating gas (4.6mL with with an H<sub>2</sub>

content of 48.54%). Therefore of the NiO/MoO<sub>2</sub>/MoO<sub>3</sub>/C cathode has good hydrogen evolution catalytic activity. After the calculations, Coulombic efficiencies of CP, Pt and NiO/MoO<sub>2</sub>/MoO<sub>3</sub>/C were 19.18, 73.19 and 79.11, respectively. In this case, NiO/MoO<sub>2</sub>/MoO<sub>3</sub>/C shows better hydrogen production performance than Pt.

### 3.4 NiO/MoO<sub>2</sub>/MoO<sub>3</sub>/C stability test

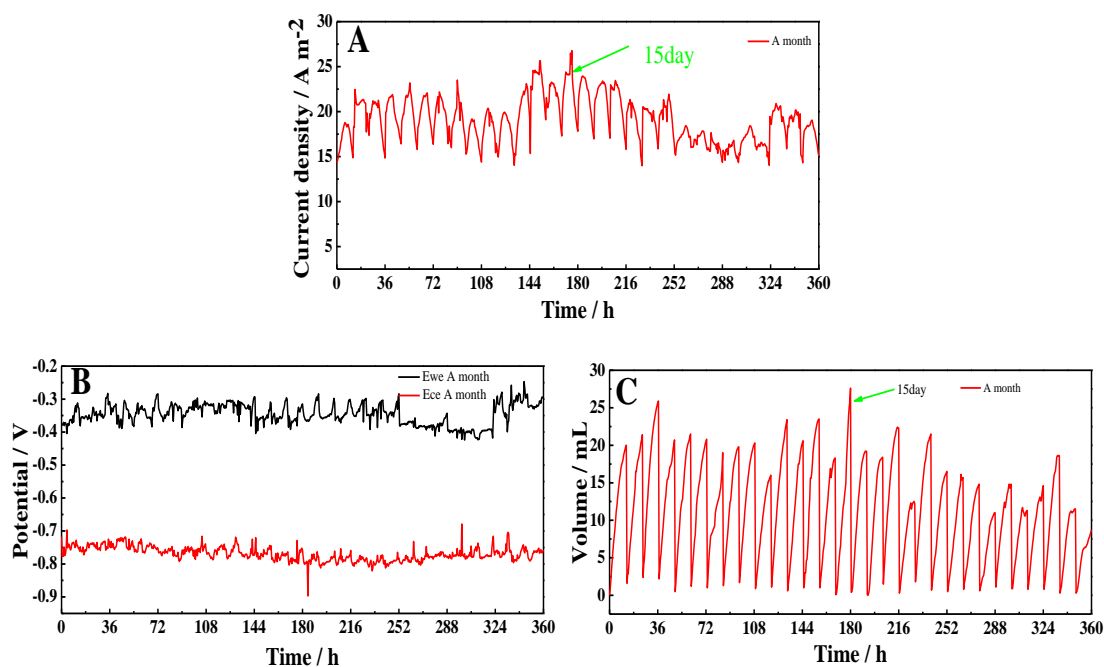


**Figure 5.** Current density variation with time (A), anode and cathode potential variation with time (B) and generated hydrogen volume variation with time in MEC (C).

The current, anode and cathode potentials and the volume of hydrogen were recorded every 30 minutes, and the nutrient solution was replaced in a 24 h cycle to investigate the stability of the long-term operation. Figure 5A shows that the current density in each cycle slowly increased to its highest level and then slowly decreased. The current density peaked on the 15th day, decreased and then gradually increased. Figure 5B shows the relationship between the cathode and anode potentials as a function of time. The average potential of the anode was  $-0.30\text{V}$ , the average potential of the cathode was  $-0.75\text{V}$  and the potential difference between the cathode and anode was  $0.45\text{V}$ . The fluctuation range of the potential during the whole operation was relatively small, and the anode and cathode potentials were relatively stable. The applied voltage was  $0.7\text{V}$  and the potential difference was  $0.45\text{V}$ , mainly due to the internal resistance of the solution and the presence of electrode polarisation. Figure 5C shows the volume of hydrogen produced as a function of runtime. During each cycle, the amount of gas gradually increased with time, the gas generated on the 15th day reached  $27.6\text{ mL}$  and the generated current was the largest. After 15 days, the gas volume was reduced. The average volume of the entire process gas was  $19.58\text{ mL}$ .

#### 4. CONCLUSIONS

After electrodepositing Mo/Ni on a carbon paper substrate via cyclic voltammetry NiO/MoO<sub>2</sub>/MoO<sub>3</sub>/C was obtained, owing to its lamellar nanostructure. The composite showed a better hydrogen production performance than Pt and demonstrated good stability.

#### ACKNOWLEDGEMENTS

This work was funded by the Provincial Natural Science Foundation of Shanxi Province, China (2014011014-6, 201701D121028). The authors also acknowledged the Institute of Coal Chemistry, Chinese Academy of Sciences for technical assistance.

#### References

1. D. Call, B. E. Logan, *Environ sci technol*, 42 (2008) 3401.
2. S. K. Cho, M. E. Lee, W. Lee, Y. Ahn, *Int. J. Hydrogen Energy*, 44 (2019) 2253.
3. K. J. Chae, M. J. Choi, K. Y. Kim, F. F. Ajayi, I. Chang, I. Kim, *Environ sci technol*, 43 (2009) 9525.
4. M. F. Manuel, V. Neburchilov, H. Wang, S. R. Guiot, B. Tartakovsky, *J. Power Sources*, 195 (2010) 5514.
5. P. A. Selembo, M. D. Merrill, B. E. Logan, *Int. J. Hydrogen Energy*, 35 (2010) 428.
6. F. Li, W. Liu, Y. Sun, W. J. Ding, S. A. Cheng, *Int. J. Hydrogen Energy*, 42 (2017) 3641.
7. H. Hu, Y. Fan, H. Liu, *Int. J. Hydrogen Energy*, 34 (2009) 8535.
8. H. Hu, Y. Fan, H. Liu, *Int. J. Hydrogen Energy*, 35 (2010) 3227.
9. A. Laszczyńska, J. Winiarski, B. Szczygieł, I. Szczygieł, *Appl. Surf. Sci.*, 369 (2016) 224.
10. Y. Z. Lu, Y. Y. Jiang, W. T. Wei, H. B. Wu, M. M. Liu, L. Liu, W. Chen, *J. Mater. Chem.*, 22 (2012) 2929.
11. M. M. Liu, W. Chen, *Nanoscale*, 5 (2013) 12558.
12. W. H. Hu, X. Shang, G. Q. Han, B. Dong, Y. R. Liu, X. Li, Y. M. Chai, Y. Q. Liu, C. G. Liu, *Carbon*, 100 (2016) 236.
13. Y. Yan, X. M. Ge, Z. L. Liu, J. Y. Wang, J. M. Lee, X. Wang, *Nanoscale*, 5 (2013) 7768.
14. S. Y. Zhao, C. X. Li, L. P. Wang, N. Y. Liu, S. Qiao, B. B. Liu, H. Huang, Y. Liu, *Carbon*, 99 (2016) 599.
15. Z. Y. Yu, C. C. Lang, M. R. Gao, Y. Chen, Q. Q. Fu, Y. Duan, S. H. Yu, *Energy Environ. Sci.*, 11(2018) 1890.
16. L. Singh, R. Kumar, A. W. Zularisam, F. I. Hai, *Bioresource Technol.*, 220 (2016) 537.
17. M. R. Gao, J. X. Liang, Y. R. Zheng, Y. F. Xu, J. Jiang, Q. Gao, J. Li, S. H. Yu, *Nat. commun.*, 6 (2015) 5982.
18. Y. Wang, Y. Zhao, A. Wu, Z. Dong, J. Li, J. Wang, *Int. J. Electrochem. Sci.*, 13 (2018) 10848.
19. H. Dai, H. Yang, X. Liu, X. Jian, Z. Liang, *Fuel*, 174 (2016) 251.